UC Davis
UC Davis Previously Published Works

Title

Cluster-Dependent Charge-Transfer Dynamics in Iron—Sulfur Proteins

Permalink

https://escholarship.org/uc/item/5fp3x33z

Journal

Biochemistry, 57(6)

ISSN

0006-2960

Authors

Mao, Ziliang

Liou, Shu-Hao

Khadka, Nimesh

et al.

Publication Date

2018-02-13

DOI

10.1021/acs.biochem.7b01159

Peer reviewed

Cluster Dependent Charge-Transfer Dynamics in Iron-Sulfur Proteins

Ziliang Mao[†], Shu-Hao Liou[†,‡], Nimesh Khadka[⊥,§], Francis E. Jenney Jr.[∥], David B. Goodin[†], Lance C. Seefeldt[⊥], Michael W. W. Adams[#], Stephen P. Cramer[*,†], Delmar S. Larsen[*,†]

[†]Department of Chemistry, University of California Davis, One Shields Avenue, Davis, California, 95616, United States

[∥]Georgia Campus, Philadelphia College of Osteopathic Medicine, Suwanee, Georgia 30024, United, States

[⊥]Department of Chemistry and Biochemistry, Utah State University, 0300 Old Main Hill, Logan, Utah, 84322, United States

[#]Department of Biochemistry, The University of Georgia, Athens, Georgia 30602, United States

Abstract

Photo-induced charge-transfer dynamics and the influence of cluster size on the dynamics were investigated using five iron-sulfur clusters: the 1Fe-4S cluster in *Pyrococcus furiosus* rubredoxin, the 2Fe-2S cluster in *Pseudomonas putida* putidaredoxin, the 4Fe-4S cluster in nitrogenase iron protein, and the 8Fe-7S P-cluster and the 7Fe-9S-1Mo FeMo cofactor in nitrogenase MoFe protein. Laser excitation promotes the iron-sulfur clusters to excited electronic states that relax to lower states. The electronic relaxation lifetimes of the 1Fe-4S, the 8Fe-7S, and the 7Fe-9S-1Mo clusters are in the picoseconds timescale, although the dynamics of the MoFe protein is a mixture of the dynamics of the later two clusters. The lifetimes of the 2Fe-2S and the 4Fe-4S clusters, however, extend to several nanoseconds. A competition between reorganization energies and density of electronic states (thus electronic coupling between states) mediates the charge-transfer lifetimes, with the 2Fe-2S cluster of Pdx and the 4Fe-4S cluster of Fe protein lying at the optimum leading to them having significantly longer lifetimes. Their long lifetimes make them the optimal candidates for long-range electron transfer and as external photosensitizers for other photo-activated chemical reactions like solar hydrogen production. Potential electron-transfer and hole-transfer pathways are proposed that possibly facilitate these charge transfers.
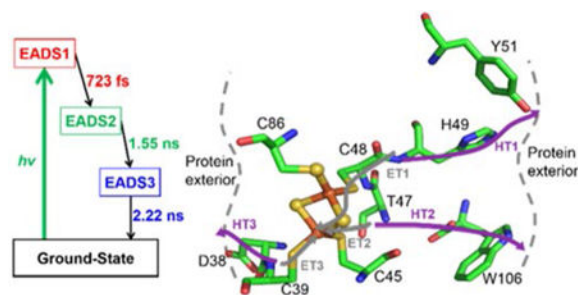
Graphical Abstract

[*]**Corresponding Authors** dlarsen@ucdavsi.edu & spjcramer@ucdavis.edu.
[‡]Max Planck Institute for Biophysical Chemistry, Am Fassberg 11, Göttingen 37077, Germany
[§]Department of Pharmacology, Case Western Reserve University, Cleveland, Ohio 44106, United States

Introduction

Iron-sulfur (FeS) clusters are ubiquitous in biology and serve not only as powerful electron-transfer (ET) agents and structural components for metalloenzymes, but also act as catalysts in their own right.[1] They are involved in many biological processes that are essential to life on earth - photosynthesis, cellular respiration and nitrogen fixation to name a few.[2] The complexity of FeS clusters ranges widely from simple clusters with a single iron atom like the rubredoxin protein from *Pyrococcus furiosus*[3] (*Pf*Rd) to complex multiple iron clusters involving additional transition metal atoms like the 7Fe-9S-1Mo cofactor from molybdenum-dependent nitrogenase (Mo nitrogenase).[4] Since the importance of FeS proteins was recognized, many techniques, such as electron paramagnetic resonance spectroscopy,[5] resonance Raman,[6] and X-ray crystallography,[7] have been applied to the study of these proteins. Despite the wealth of spectroscopic, kinetic and theoretical studies for decades, many aspects of FeS proteins are still poorly understood.

The ability to effectively and economically couple light absorption into productive outputs will be critical in the upcoming years for our developing economy. Of which, nitrogen fixation and hydrogen generation have garnered great interest and been extensively explored.[8, 9] Recently, interest about photo-induced chemical processes involving FeS proteins has grown. For instance, FeS clusters have been reported to participate in photosensitization in living cells[10]. They also take part inphoto-induced charge transfer (CT) in the purple phototroph *Rhodoferax fermentans*.[11] External photosensitizers have also been incorporated into hydrogenase and nitrogenase enzyme systems to enable photo-activated hydrogen production and nitrogen fixation.[8, 9, 12] Thus, FeS proteins and model compounds of FeS complexes have the potential to facilitate solar hydrogen and fuel production as external photosensitizers. While the light-induced dynamics of charge insertion in FeS complexes has been the focus of many studies,[10, 11, 13, 14] the photodynamics induced by direct excitation of these important complexes is largely unknown. The directly excited photodynamics is important because it provides essential information about their photochemical properties and how to better utilize these complexes in light-induced CT processes.

Rubredoxins are small, redox-active proteins that contain one iron atom that is coordinated in a tetrahedral geometry to the sulfur atoms of four cysteinyl residues (Figure 1A). They are the smallest FeS ET proteins with typically 45–55 amino acids and are found in several anaerobic bacteria.[15] Their roles differ from organism to organism, involving electron transfer in acetogenesis[16] and reduction of nitrate,[17] alkane oxidation[18] and superoxide

reduction.[19] The rubredoxin from the hyperthermophilic archaeon *Pyrococcus furiosus* (*Pf*Rd) is extremely stable, with an unfolding rate of ~10^{-6}s^{-1} at 100 °C.[20] It has been a model for studying thermal stability of hyperthermophilic proteins. Its crystal structure has been determined by both X-ray diffraction and NMR spectroscopy (Figure 1A).[3] In this study, the CT dynamics of *Pf*Rd is compared to the dynamics of other proteins that contain multinuclear iron clusters to investigate the cluster dependence of their electronic relaxation dynamics.

2Fe-2S ferredoxins are small FeS proteins with 90–130 amino acids and contains a single $Fe_2S_2(S\text{-}Cys)_4$ redox center. Most 2Fe-2S ferredoxins are ET proteins, among which the putidaredoxin (Pdx) from *Pseudomonas putida* is one of the most studied. Previously, we reported the ultrafast CT dynamics in the 2Fe-2S complex of *Rhodobacter capsulatus* ferredoxin VI (Rc6).[21] Here, we extend our study to Pdx and compare with other FeS proteins. Pdx serves as a one-electron mediator from NADH-dependent putidaredoxin reductase (Pdr) to oxygenase cytochrome P450cam in the three-component camphor hydroxylase system.[22] X-ray crystal structures of both Rc6 and Pdx (Figure 1B)[7, 23] exhibit almost the same active site structures (Figure S6). Protein BLAST[24] performed on both proteins (PDB codes: 1E9M for Rc6, 1PUT for Pdx) shows that these two proteins have 41% identity and 66% similarity with an expectation value of 4×10^{-33}, which all indicate that these two proteins are highly similar to each other.

4Fe-4S clusters are important ET agents in ferredoxins,[25] high potential proteins (HiPIPs),[11] nitrogenases[26] and hydrogenases.[27] In these proteins, the cubane 4Fe-4S unit is usually coordinated by four cysteines. The oxidation states of the 4Fe-4S clusters in ferredoxins and nitrogenase iron proteins usually cycle between [4Fe-4S]$^{1+}$ and [4Fe-4S]$^{2+}$, with their reduction potentials typically ranging from −700 to −300 mV.[28] In this study, the electronic relaxation dynamics of the 4Fe-4S cluster in nitrogenase iron protein are compared to the other FeS clusters, including the 8Fe-7S and 7Fe-9S-1Mo clusters also used by nitrogenase. Nitrogenase is the enzyme that catalyzes the conversion of dinitrogen in the air to ammonia in biological nitrogen fixation processes. It is able to break the dinitrogen triple bond under ambient temperature and atmospheric pressure and constitutes ~50% of the global nitrogen fixation annually. However, despite over 50 years of study on nitrogenase, aspects of its catalytic mechanism remain poorly understood. Even which atom on the nitrogenase active site that the dinitrogen molecule initially bind to is debated.[26]

Among the different types of nitrogenases, the Mo-nitrogenase is the most common. It is constituted of two component proteins: the Fe protein which contains a 4Fe-4S cluster (Figure 1C) and the MoFe protein that contains a 8Fe-7S P-cluster (Figure 1D) and a 7Fe-9S-1Mo cofactor (FeMoco, Figure 1E). During nitrogenase turnover, electrons transfer from the Fe protein 4Fe-4S cluster to the P-cluster of the MoFe protein and then to the FeMoco, where substrates are reduced (Figure 2). Photolysis studies on CO-inhibited nitrogenase identified several ligand binding schemes that might be important for nitrogen turnover.[29, 30] Recently, King et al. successfully incorporated an external photosensitizer to direct photo-activated ET from artificial external nanorods to the MoFe protein to facilitate nitrogen fixation.[9] However, the photodynamics inducing CT reactions of nitrogenase Fe and MoFe proteins have never been studied in detail. The knowledge of the photochemistry

of the FeS clusters in Fe and MoFe proteins is helpful in the design of photo-induced nitrogenase mutants/nitrogen fixation devices. It will also aid in the understanding of the photolability of ligand-bound nitrogenase, from which information about dinitrogen binding on the FeMoco can be inferred.

Recently, we reported the ultrafast electronic dynamics of the 2Fe-2S Rc6 characterized using ultrafast transient absorption (TA) spectroscopy.[21] In this paper, we extend the study on Rc6 to the above-mentioned FeS proteins that contain 1-Fe, 2-Fe, 4-Fe, 7-Fe and 8-Fe clusters using ultrafast TA spectroscopy. The TA spectroscopy directly measures the excited-state population evolution, electron transfer and intersystem crossing, etc. We aim to characterize and ultimately direct critical CT dynamics in these systems. The information about ultrafast electronic dynamics in these FeS complexes will provide useful information in the utilization of these complexes in photo-induced ET or photosensitization processes, as well as in the design of model complexes that can be used for these purposes.

Materials and methods

Protein Purification and Sample Preparation

***Pf*Rd:** Recombinant *Pf*Rd (N-met form) was purified as described in Jenney and Adams 2001,[15] except that the protein was expressed from a pET24d derived plasmid (pETPfRd1). Plasmid pET24d was digested with *Nco*I and *Bam*HI. The rubredoxin encoding gene (PF1282) was amplified by PCR from Pyrococcus furiosus genomic DNA with *Nco*I and *Bam*HI sites added at the N and C terminii, respectively, and was cloned in frame with the translation start site of pET24d, resulting in plasmid pETPfRd1.The protein was concentrated in 50 mM Tris pH 8.0 / 400 mM NaCl to 52 mg/ml for shipping and flash frozen in liquid nitrogen for storage.

Pdx: The pET-Pdx plasmid was constructed by the pET vector with Pdx as the insert.[23] It was transformed into BL21 (DE3) and grown in 17×100 mm culture tube in 6 ml LB broth (Luria-Bertani broth) and 100 mg/ml ampicillin for 8 hours at 37 °C. The cultures were then transferred to 4×1L TB (Terrific Broth) broth containing 100 mg/ml ampicillin. After growth at 37 °C for 12 hours, cultures were induced with 0.4 mM IPTG (Isopropyl β-D-1-Thiogalactopyranoside), and the temperature was dropped to 30 °C for 24 hours. Cells were resuspended in 100 ml 50 mM potassium phosphate (pH=7.5) before being lysed by a French Press. After centrifugation to remove the cell debris, the lysate was applied to a DEAE-anion exchange column (DEAE Sepharose Fast Flow, GE Healthcare), eluted with a salt gradient of 30–270 mM KCl in 840 ml, and fractions with $A_{412}/A_{280} > 0.1$ were concentrated and loaded to a 1.8 L Sephacryl S-200 size exclusion column. The fractions with $A_{412}/A_{280} > 0.48$ were collected for later experiments. The Pdx protein was studied in the oxidized form.

Nitrogenase MoFe and Fe proteins: All reagents were purchased from Sigma Aldrich (St.Louis, MO) or Fisher Scientific (Fair Lawn, NJ) unless otherwise stated and used without further purification. *Azotobacter vinelandii* strains DJ995 (wild-type) was grown, and the corresponding nitrogenase wild-type MoFe proteins having a seven-His tag addition near the carboxyl-terminal end of the α-subunit was expressed and purified as previously

described.[31] The Fe protein does not have a poly-His tag and was purified from wild-type *Azotobacter vinelandii* cells using previously published methods.[30] Protein concentration was determined by the Biuret assay using bovine serum albumin as standard. The proton reduction (2100 nmol/mg/min) and acetylene reduction (2010 nmol/mg/min) enzymatic activity for the purified wild-type MoFe protein was determined using Fe protein as an immediate electron donor in the MoFe:Fe ratio of 1:20 (0.1 mg MoFe protein and 0.5 mg Fe Protein) using an activity assay protocol described before.[32] All handling of proteins and buffers was done in septum-sealed serum vials under an argon atmosphere or on Schlenk vacuum line.

Ultrafast Spectroscopy

The ultrafast TA system used for this study has been described previously.[33] An amplified Ti:sapphire laser system (Spectra Physics Spitfire Pro and Tsunami) generated 1 kHz repetition rate pulses at 800 nm wavelength and 2.5 mJ energy, with a full width at half-maximum of 40 fs. The laser beam was split into three separate paths for the generation of excitation (pump) and probe pulses respectively. The 400 nm excitation pulses used for exciting *Pf*Rd, nitrogenase Fe protein and nitrogenase MoFe protein were produced through second harmonic generation (SHG) by focusing a part of the 800 nm light into a β-barium borate (BBO) crystal. The 490 nm excitation wavelength was selected for Pdx to simultaneously excite the CT transitions to iron from the opposite cysteine sulfur, the nearby cysteine sulfur, and the bridging sulfide of the 2Fe-2S cluster.[34] The 490 nm excitation pulses were generated with a home-built, noncolinear optical parametric amplifier (NOPA) that was pumped by the SHG of the 800 nm beam in another BBO crystal and seeded by a white light supercontinuum produced in a thin plate made of yttrium aluminum garnet (YAG). Another femtosecond white-light continuum (350–715 nm) was generated by focusing a portion of the fundamental 800 nm pulse (~500 nJ) into a slowly translating 2 mm CaF2 crystal for broadband probing. The angle between the polarization of the excitation and probe pulses was set at 54.7° (magic angle) with respect to each other to eliminate anisotropic effects associated with rotational dynamics. After passing through the sample, the probe light was dispersed by an imaging spectrograph (Oriel MS 127i) to a 256-pixel photodiode array (Hamamatsu S3901 and C7884). The excitation pulses were chopped at 500 Hz so that difference spectra between the excited and un-excited samples can be collected. The time delay (−10 ps to 7.5 ns) between the excitation and probe pulses was controlled by mechanically delaying the probe pulses using a computer-controlled linear motor stage (Newport IMS 600). The instrumental response for the experiment was ~150 fs.

The *Pf*Rd and Pdx samples were continuously flowed through a 2-mm pathlength quartz cuvette using a peristaltic pump (Watson Marlow 401U/D) to ensure replenishment of new samples between successive laser shots (1 ms). The nitrogenase Fe protein and MoFe protein samples were loaded into 1-mm pathlength quartz cuvettes (Spectrocell Inc., R-4001-T) inside a glovebox with less than 2 ppm oxygen and tightly capped by applying vacuum grease on the threads. The cuvettes were then brought out of the glovebox and immediately sealed with low temperature wax around the caps to further eliminate the possibility of oxygen entering the cuvettes. Two high speed motorized actuators (Newport LTA-HS, controlled by a Newport ESP 300 Motion Controller) were used to translate the sample

cuvettes (3 Hz, 1 cm translation distance in both x and y axes) across the laser beam[35] to avoid excessive exposure of the samples to multiple laser shots. The absorbance of all four samples was set between 0.15 OD and 0.7 OD at their respective excitation wavelengths. UV-visible absorption spectra were measured before and after the laser experiments and no significant change to the samples was observed.

Results

The steady-state absorption spectra together with the excitation laser spectra for all four proteins are shown in Figure 3. The spectra of the *Pf*Rd and Pdx are typical of oxidized rubredoxin[3] and 2Fe-2S ferredoxins, respectively.[23] While the oxidized Pdx exhibits no clearly-resolved absorption bands in the longer wavelength region (> 465 nm, Figure 3B), there are multiple CT transition bands of different characters buried in that region as predicted with quantum calculations by Noodleman[34] and Sharma.[36] Therefore, the pump laser at 490 nm will excite multiple CT transitions simultaneously. The spectra of both nitrogenase Fe protein and MoFe protein are relatively featureless with absorption decreasing monotonically from near ultraviolet region to longer wavelength. This indicates sample integrity during sample preparation because for both proteins distinctive features appear upon oxygen exposure.[37, 38] Specifically, a shoulder at ~435 nm will appear in the steady-state absorption spectrum of MoFe protein,[37] while for the Fe protein, absorption will increase in the region from 400 nm to 650 nm.[38] Steady-state absorption spectra taken for all the four proteins after the TA experiments showed no change in the spectra and confirm that sample integrity was preserved during the ultrafast TA experiments. For the Fe protein, the steady-state spectrum displays the characteristic feature of an oxidized $[4Fe-4S]^{2+}$ cluster because upon reduction the absorption in the 350 – 700 nm range will decrease (Figure S8).[39]

The TA spectra at select times and kinetics at select wavelengths of *Pf*Rd are compared in Figure 4. Immediately following laser excitation, the TA spectra at the wavelength region shorter than 610 nm largely resembles the steady-state difference spectrum of reduced – oxidized *Pf*Rd (Figure 9A), which suggests a transient reduction of the active site metal cluster induced by laser-induced LMCT. A broad positive excited-state absorption (ESA) band at around 650 nm forms within 200 fs after laser excitation. After that, the ground-state bleach (GSB) band at around 493 nm and the ESA band at around 625 nm decay slowly with a similar rate (Figure S7) and persists beyond 60 ps, which indicates they may represent the same intermediate species or two species that are in equilibrium. The 675 nm band decays away faster than that of 625 nm (Figure S7), indicating a different species. The two positive bands at around 430 nm and 540 nm form transiently (within 1 ps) and then decays away within 5 ps. The TA spectra and kinetics for Pdx are shown in Figure 5. It shows essentially the same spectral features and kinetics as Rc6,[21] except that the early kinetics (before 200 fs) are obscured by cross phase modulation[40,41] (CPM) artifacts and stimulated Raman effects of water in the buffer solution,[42] manifested by the sharp rising and decaying phase in the early kinetics. This shows that the two 2Fe-2S ferredoxins share similar excited-state dynamics probably because they share highly similar active site structure (Figure S6; 41% identity and 66% similarity with an expectation value of 4×10^{-33}).

The spectral features of *Pf*Rd share similar features as that of the Pdx and Rc6, exhibiting positive ESA bands at around 430 nm, 540 nm and 650 nm and a GSB band around 490 nm. However, the ESA bands at 430 nm and 540 nm are short-lived compared to that of Pdx and Rc6. The kinetics of *Pf*Rd are very different from that of Pdx and Rc6. While the kinetics of *Pf*Rd only lasts for a few tens of picoseconds, that of Pdx and Rc6[21] persists up to 7.2 ns.

Both nitrogenase Fe protein (Figure 6 A,C) and MoFe protein (Figure 7 A,C) show very distinct transient spectral features from that of *Pf*Rd (Figure 4 A,C) and Pdx (Figure 5 A,C) with no obvious GSB band in the 410–700 nm probing window. Although both nitrogenase Fe and MoFe proteins share somewhat similar TA spectral features, there are differences as well. The TA spectra of the Fe protein clearly show three bands with different kinetics: (a) The short-lived positive band at around 575 nm that decays away within 500 fs; (b) The positive band at around 440 nm that persists up to 10 ps; (c) A positive band at around 650 nm that persists up to 7.2 ns. This suggests that there are at least three different populations in the Fe protein electronic relaxation kinetics. However, the TA spectra of the MoFe protein suggests mainly two obviously distinct bands/species: one at around 650 nm and the other around 475 nm, with the 650 nm band decaying faster than the 475 nm band.

The electronic relaxation kinetics of the nitrogenase Fe (Figure 6 B,D) and MoFe (Figure 7 B,D) proteins display the most striking differences. The Fe protein transient kinetics persist beyond 7.2 ns and is slightly longer than that of Pdx, whereas the transient difference spectra of the MoFe protein decays to zero within a few tens of ps and more closely resembles *Pf*Rd (Figure 4). For the Fe protein, the positive band on the blue side (~440 nm) decays faster than the positive band on the red side (~650 nm) of the spectra, whereas for the MoFe protein, the positive band on the blue side (~450 nm) seems to decay slightly slower than the band at the red side (~650 nm), at least in the time scale within 2 ps.

Global Analysis

We adopt a multi-compartment global analysis method to simulate the data and try to unravel the underlying spectral species and their corresponding kinetics. The global analysis methodology has been described in detail before.[43, 44] To summarize, the TA data are decomposed into a set of distinct species or populations with time-independent spectra and time-dependent populations (i.e., population evolution profiles) according to a postulated model. This can be implemented numerically by fitting the data to a system of linear first-order differential equations (eq. 1):

$$\frac{dn_i}{dt} = A_i I(t) + \sum_{i,j} K_{ij} n_i$$

(1)

In these equations, n_i represents the ith species or population with time-independent spectrum, A_i represents the initial occupancy of the ith species, $I(t)$ is the excitation pulse

temporal profile, and K is the matrix that describes the connectivity scheme between the underlying spectral species or populations in the postulated model, with Kij being the time constant of evolution from the ith population to the jth population.

There are different global analysis models depending on the postulated connectivity schemes. One that is widely used for the fit of photodynamics is called sequential model, where the populations are assumed to evolve from an initial population/species consecutively to the subsequent ones (A → B → C → …). The extracted difference spectra using the sequential model are thus termed evolution-associated difference spectra (EADS). When the postulated model accurately describes the underlying photodynamics, the extracted difference spectra are also called species-associated difference spectra (SADS) and represent the true difference spectra of the constituent species in the system of interest. Otherwise, the extracted spectra do not represent the true spectra of the underlying species, but are linear combination of the true SADS. Nevertheless, the EADS analysis provides useful information to help unravel the underlying spectral evolution and associated directly observed time scales. It also provides insights for the construction of proper target models, although none were attempted here. Sequential model analysis on the ultrafast transient dynamics of the 2Fe-2S cluster in Rc6 successfully revealed multiple states evolving from higher excited states to lower ones.[21] Considering that the four proteins that are surveyed in this paper all contain FeS clusters, sequential model analyses suffice in describing the ultrafast electronic dynamics in these proteins as well.

As mentioned above, direct observation of the TA data suggests that there are at least two different species in the kinetics of *Pf*Rd and MoFe protein, and at least three intermediate species in the Pdx and Fe protein data. The sequential analyses performed on the four proteins (Figure 8) used at least three compartments (Figure 8) and fit their respective TA data well (panels B and D of Figures 3–6). One obvious observation from the sequential analyses is that the EADS for all the four proteins share similar spectral features with the TA spectra of each protein. For example, the EADS2 of *Pf*Rd (Figure 8A) is similar to the TA spectrum of *Pf*Rd at 1 ps (Figure 4A) while all the three EADS for Pdx (Figure 8C) resemble its TA spectra (Figure 5). The same is true with nitrogenase Fe and MoFe proteins. While the EADS for *Pf*Rd and Pdx (Figure 8 A,C) may not be so obvious to observe from the raw TA data (Figure 4,5), the EADS of nitrogenase Fe and MoFe proteins (Figure 8 E,G) can be easily identified even by merely looking at the raw transient data (Figure 6,7) and are thus closer to the true underlying photodynamics. Specifically, from the raw TA data of the nitrogenase Fe protein, it can be easily perceived that there is a band at around 575 nm that forms instantaneously upon laser excitation and decays away within 1 ps, leaving two positive bands at around 450 nm and 650 nm that decay in longer time scale, with the 650 nm one persists all the way to the end. For the MoFe protein, it is not difficult to identify the two positive bands at around 460 nm and 650 nm, with the 650 nm band decaying faster than the 460 nm one. The third EADS in the MoFe EADS analysis is not very obvious to observe directly from the raw data. However, its presence is essential for the fit of the "dip" around 5 ps in the transient kinetics at 445 nm and 500 nm and thus reveals that there is a relatively long lifetime (~25.2 ps) and weak population present in the kinetics. The "ripples" at around 460 nm in EADS1 and EADS2 of *Pf*Rd probably arise from the water Raman

peak.[42] It only exists within the first 200 fs and is not interesting/relevant in the present study and thus can be ignored.

The EADS for Pdx are nearly identical to the EADS previously reported for Rc6.[21] The only difference is that only three EADS are presented here for Pdx because a shorter-lived EADS (EADS S3 in Figure S3) is obscured by the strong CPM artifacts[40, 41] and stimulated Raman signal of water,[42] and it is difficult to extract useful information about the short-lived species in the data. Its lifetime (143 fs) is also slightly shorter than the instrumental response and thus not accurate. The details of the complete EADS analysis of Pdx with the short-lived EADS are presented in the Supporting Information (Figure S3).

Discussion

In the following sections, the CT dynamics in *Pf*Rd, Pdx, and nitrogenase Fe and MoFe proteins are first discussed individually, and then a comparison of their dynamics is made to try to unravel the factors that mediate their different dynamics.

P. furiosus Rubredoxin

*Pf*Rd is the simplest form of FeS proteins with a mononuclear iron center coordinated with four cysteinyl sulfurs. The electronic dynamics observed in *Pf*Rd in the present study is consistent with the extensive studies conducted by Kennepohl and Solomon on the electronic structure contributions to ET in 1Fe-4S clusters from *Desulfovibrio vulgaris* rubredoxin (*Dv*Rd) and in model complexes with a FeX4 cluster (where X can be a chloride or cysteinate thiolate).[45–47] They used a series of experimental and theoretical methods, including photoelectron spectroscopy, density functional methods, and model compound studies, to investigate the effect of electronic relaxation on ET, the reduction potential of 1Fe-4S clusters, and the kinetics of ET in 1Fe-4S proteins.

The present study on *Pf*Rd reveals three different populations involved in the photodynamics with lifetimes of 279 fs, 456 fs and 2.37 ps. The first characteristic of these lifetimes is that they are all very short, which is consistent with the experimentally observed and theoretically predicted fast ET rate in rubredoxin,[48, 49] as well as the short lifetime observed in ICVS study of *Pf*Rd.[50] Figure 9A shows that the TA spectrum of *Pf*Rd at 215 fs largely resembles the difference absorption spectrum of *Pf*Rd obtained by subtracting the oxidized spectrum from the reduced spectrum. This suggests that the EADS1 (279 fs) might involve a transient "internal" reduction of the active site through LMCT induced by the excitation laser. According to Kennepohl and Solomon,[45] the electronic relaxation in 1Fe-4S sites due to increased LMCT is responsible for significant stabilization of the oxidized state, which may explain the transient nature of the "internal" reduction upon laser excitation. The electronic relaxation observed in 1Fe-4S clusters was also found through density functional studies to reduce both the inner-sphere reorganization energy and the electronic coupling matrix element, with the former effect dominating.[46] The large decrease of the inner-sphere reorganization energy results in an increase of the overall ET rate by 3 orders of magnitude, [46] which explains the extremely short electronic relaxation lifetimes in *Pf*Rd observed in this study.

The short lifetimes also suggest that there is probably no long-range photo-induced ET pathways in *Pf*Rd as was proposed in Rc6,[21] because both the short lifetimes observed in this study and the fast electron self-exchange rate observed experimentally[49] do not support long-range ET. Considering that the active site of *Pf*Rd is close to the surface of the protein, especially that CYS8 and CYS41 (they are Cys9 and Cys 42 respectively in *Dv*Rd) are exposed to protein exterior, this makes sense because a long-range pathway is not necessary for *Pf*Rd to exchange electrons with its redox partners. However, since the surface exposure of the active site is very small (0.4% in *Dv*Rd) even including the regions within three sigma-bonds from the active site (3.2% in *Dv*Rd),[46] it probably either requires a precise docking mechanism for rubredoxin to participate in ET with redox partners or there might be some slightly longer ET pathways that extend to the surface areas a little farther away from the active site, such as those through the sulfur H-bonds of the cysteinate sulfurs to the surface amide oxygens (~4 sigma-bonds from the active site)[46] as described below.

Despite the lack of long-range ET paths, several potential short ET pathways in *Pf*Rd have been proposed. Besides a solvent mediated ET pathway through the proximal cysteines suggested by molecular dynamics simulations,[48] Kennepohl and Solomon proposed two major ET pathways in *Dv*Rd by employing a simple Beratan-Onuchic model to estimate the propagation of electrons through the protein matrix.[46] One is a shorter path through the β-methylenes of the surface cysteinate ligands (Cys9 and Cys42). The other is through the sulfur hydrogen bonds of the cysteinate sulfurs to the surface amide oxygens, such as those of Thr7, Val8, Gly10, Pro40, Val41 and Gly43, because the hydrogen bonds can create additional paths to the protein surface and significantly increase the surface area through which the active site can interact with its redox partners. So there are at least three potential ET pathways, with two of them of shorter lengths (within two σ-bonds) and the other one with slightly longer distance (up to four σ-bonds). Considering all the discussions above, the excitation laser induced a transient internal reduction of the 1Fe-4S site, probably through one or multiple of the short-range ET pathways described above, which rapidly relaxes back to the original unexcited state due to the small reorganization energy of the cluster.

P. putida putidaredoxin

Pdx is the second smallest FeS protein investigated in this study, with a 2Fe-2S cluster as the active site. Although the overall kinetics of Pdx and Fe protein both persist up to 7 ns, Pdx has two long-lived populations with comparable lifetimes of 1.55 ns and 2.22 ns and potentially compete each other, whereas the lifetimes of the three EADS of the Fe protein are more distinct with only one long-lived state. The two long-lived populations in Rc6 with a similar 2Fe-2S cluster were attributed to two different ET pathways, both of which are within 3 sigma-bonds (within 5 Å) because the electronic decay was within 8 ns.[21] The longer-lived state suggests a potentially longer-range "external" ET pathway from a surrounding amino acid to the cysteinyl sulfur of the active site, and eventually to the iron atom opposite to the cysteine sulfur. The other shorter-lived state possibly indicates the existence of a transient "internal" shorter-range ET from the nearby cysteinyl sulfur or the bridging sulfide to one of the iron atoms in the active site. Considering the close structural homology of Rc6 and Pdx, the two long-lived states in Pdx may also arise from similar "external" and "internal" ET pathways. The longer-lived EADS3 of Pdx resembles its

reduced - oxidized difference absorption spectrum (Figure 9B), suggesting a potential photo-induced "external" ET from a surrounding amino acid to the 2Fe-2S cluster upon laser excitation. Where the shorter-lived EADS2 is similar to EADS3, it also contains an additional positive band at around 650 nm that is similar to Rc6.[21] Therefore, it is reasonable to assign the two long-lived states in Pdx to similar longer and shorter ET pathways as in Rc6 (Scheme 1: ET1 for the longer-ranged ET, ET2 or ET3 for the shorter-range ET).

The possible existence of the longer-range "external" ET pathway in Rc6 was further supported by the existence of hole-transfer (HT) pathways in the protein matrix to quench the electron holes created by the ET process. A similar search was made in Pdx to identify potential HT pathways. Tyrosine and tryptophan residues have been reported to participate in long-range HT in proteins because of their lower redox potential due to the change of their protonized states.[51] Therefore, the crystal structure of Pdx was examined to identify possible tyrosine and/or tryptophan chains that are connected to the ET pathways. However, only those residues that lead to the protein exterior or the Pdx-Pdr and/or Pdx-P450cam interaction sites (e.g. near Trp106) are included in the search. Since Fe1 (Scheme 1) was reported to be preferentially reduced and favored for ET in plant-type and vertebrate-type 2Fe-2S ferredoxins,[52, 53] the searches were started from Fe1.

Three major HT pathways were found in this search, corresponding to the three ET pathways shown in Scheme 1. The first one follows the same pathway as was identified in Rc6.[21] It goes through Fe1 → S1 → Cys48 → His49 → Try51 → protein exterior (ET1 and HT1 in Scheme 1). The His49 is directly bound with Cys48. Its imidazole side chain is only 3 angstroms from the phenolic oxygen of tyrosine 51, which is solvent exposed. The second pathway extends through Cys45 → Thr47 → Trp106 → protein exterior (HT2 in Scheme 1). This HT pathway was not identified in Rc6. However, Sevrioukova et al.[23] has proposed a potential CT pathway in Pdx through the same route. It is coupled to the shorter-range ET pathway from Cys45 sulfur to Fe1 (ET2 in Scheme 1). According to Sevrioukova et al.,[23] the threonine was included in the CT pathway for two reasons. Firstly, Thr54 in Adx, an analogue of Thr47 in Pdx, was calculated to have the highest electron coupling value and thus more likely to be involved in ET pathways.[54] Secondly, Thr47 is hydrogen bonded to Cys45 sulfur and is partially shielded by the indole ring of Trp106, which is important in the Pdx-P450cam interaction.[55, 56] The Cys45 residue has also been predicted using Harlem[56, 57] to be involved in the ET pathway from the 2Fe-2S cluster of Pdx to the Fe atom of P450cam. Thus, this second ET pathway is very likely to participate in the photo-induced dynamics observed in this study. A third potential ET/HT pathway that may correspond to the shorter-lived population is from Fe1 to Cys39, Asp38 and then the protein exterior (ET3 and HT3 in Scheme 1) as was proposed by Roitberg et al. through combined theoretical and experimental studies.[58] A ET pathway from Pdr to Pdx that involves Cys 39 has been predicted using Harlem.[57, 59] The Cys39 and Asp38 pair has also been predicted by Harlem to be involved in the ET from the 2Fe-2S cluster of Pdx to the heme group of P450cam.[57, 59] Therefore, this pathway is also highly possible to contribute to the CT dynamics observed in the TA study.

The longer-range ET path from the opposite sulfur to iron is within 5 Å, therefore the 7 ns electronic decay time should be sufficient considering that a 25 ns ET time has been reported

for a 10 Å ET in proteins.[60] The long-range HT1 and HT2 may not occur unless coupled with external electron donors. The longer lifetimes as well as the cluster's close proximity to the protein surface also suggest that Pdx could potentially be used as photosensitizers for light-induced chemical reactions like hydrogen production in hydrogenase or hydrogenase model compounds.

Nitrogenase Fe protein

The nitrogenase Fe protein contains a 4Fe-4S cluster between its two subunits and serves as the electron donor to MoFe protein during catalytic turnover. The EADS of the nitrogenase Fe protein have several distinct features. Firstly, the EADS are all positive within the probe wavelength range, probably because the GSB band is on the blue side of the excitation laser at 400 nm and out of the probing range of the experiment. Secondly, the spectral features of the three EADS are distinct and well separated. This indicates that the three-compartment sequential model used for the fitting of the Fe protein data probably extracts and separates the underlying spectral species quite well and is likely close to the "true" model. The excitation laser promoted the sample to an excited state that subsequently evolved to two lower states, with the lowest state having a lifetime of 7 ns and eventually decayed to the ground state. Thirdly, although the kinetics of Pdx and Fe protein both persist up to 7 ns, Fe protein has only one long excited state that is 2–3 times longer than that of Pdx and Rc6. Intuitively, it might be argued that the larger 4Fe-4S cluster might have a larger reorganization energy and thus leads to slower ET rate and longer electronic relaxation lifetime. However, theoretical calculation of the inner-sphere reorganization energies for FeS clusters with 1, 2, and 4 irons found that the reorganization energies of 2Fe (36.8 kJ/mol)[28] and 4Fe (32 kJ/mol)[28, 61] clusters are very similar. Therefore, it is hard to attribute the long lifetime in 4Fe-4S cluster to increased reorganization energy. Considering that the 2.2 ns lifetime in 2Fe-2S clusters and the 7 ns lifetime in 4Fe-4S clusters is actually not that much different and that the cubic 4Fe-4S cluster can be viewed as six pairs of 2Fe-2S clusters, it is possible that the two different lifetimes in 2Fe-2S clusters are "smeared" into a longer lifetime in the 4Fe-4S cluster due to the coupling of electronic relaxations of the six "virtual" pairs of 2Fe-2S clusters.

Nonetheless, the long excited state may still indicate the existence of at least one CT pathway in Fe protein. Theoretical calculations performed by Aizman et al.[62] on $[Fe_4S^*_4(SCH_3)_4]^{2-}$ synthetic analogs assigned the 400 – 425 nm absorption band to S (3p) → Fe (3d) CT transitions. Therefore, the 400 nm excitation laser pulse promotes mostly CT transitions from the cysteinyl sulfurs to the iron atoms. Comparison of the EADS3 with the reduced – oxidized difference absorption spectrum of the Fe protein (Figure 9C) reveals that they resemble each other qualitatively, especially in the wavelength region above 500 nm. This suggests that the 400 nm pump laser is probably inducing an internal reduction of the 4Fe-4S cluster that persisted for ~ 7 ns. This is similar to what was observed in Pdx and Rc6 and is consistent with the fact that the 400 nm laser mostly promotes CT from cysteinyl sulfur to the irons. It is possible that upon laser excitation, one electron on the cysteinyl sulfur was promoted to move to the irons in the 4Fe-4S cluster, and then the electron hole of the cysteine was quenched by one or multiple HT pathways that exist in the Fe protein. This

indirect long-distance (over 10 Å) CT mechanism in FeS proteins has been suggested by Noodleman and Case as early as 1984[34, 63] and was reported in Rc6.[21]

However, not like in Rc6 and Pdx, the examination of the crystal structure of the nitrogenase Fe protein failed in finding nearby tyrosine or tryptophan chains that may participate in hole quenching processes, because the closest of these residues are more than 10 Å away from the 4Fe-4S cluster. Considering that the ET from nitrogenase Fe protein to MoFe protein requires the proper docking of these two proteins following the conformational changes induced by MgATP binding, it is possible that new ET/HT pathways between the Fe and MoFe may form after these two proteins are properly docked. Further study on this topic will help to understand the intermolecular ET between nitrogenase component proteins. Besides the implication of ET pathways, the long lifetime also makes 4Fe-4S clusters the optimal candidate among all the investigated FeS clusters for potential application as external photosensitizers for other photo-activated reactions.

P cluster and FeMoco in nitrogenase MoFe protein

The MoFe protein contains two metal clusters. One is the 8Fe-7S P-cluster and the other is the 7Fe-9S-1Mo FeMoco, with the P-cluster as the electron shuttle between nitrogenase Fe protein and the FeMoco (Figure 2). The measured TA signals of the MoFe protein are therefore a mixture of the signals from both clusters. Although the EADS analysis is a mixture of two different dynamic systems, what is clear is that the dynamics in both clusters are exceedingly fast. Both clusters also have larger sizes than the other FeS clusters investigated in this study. They also both undergo structural changes upon oxidation state changes.[64] This suggests that the P-cluster and the FeMoco may have a larger energy barrier for electron transfer as well as larger reorganization energies, which should contribute to lower ET rates and longer-excited state lifetimes.

Merely judging by the reorganization energies and the trend of increased lifetime from 1Fe to 4 Fe clusters, it seems to suggest that the excited-state lifetimes for the P cluster and the FeMoco should be the longest among all the FeS clusters investigated in this work. However, this was not the case. The reason, we think, is because of the ignorance of a second effect that larger cluster size and greater cluster complexity may have on the electronic states of MoFe protein. While the two clusters in the MoFe protein are much larger than the other three smaller clusters, their structures are also far more complex. Especially for the FeMoco, its trigonal prismatic structure, its bigger structural changes upon redox reactions,[64] and the inclusion of transition metal element in the cluster will all contribute to increased cluster complexity. The bigger size and greater complexity of the clusters will lead to greater electronic density of states (DOS) and thus stronger electronic coupling between states.[36] According to the Fermi Golden rule,[65] larger DOS and electronic coupling will lead to a larger transition rate between states. Simply looking at the dynamics of 1Fe, 2Fe and 4Fe clusters, it is tempting to conclude that larger cluster size increases the excited state lifetimes and thus makes a larger cluster a better candidate for long-range ET reactions and as external photosensitizers for photo-activated chemical reactions. However, the experimental data on MoFe protein refute this proposal and suggest that the increased DOS and thus stronger electronic coupling between states need to be considered as the

cluster size further increases. The fact that both clusters undergo structural changes upon redox should also be considered in future studies. Therefore, although large cluster size may enable P-cluster to carry out sequential two electron transfers[66] and the FeMoco to facilitate eight-electron reduction of substrates as proposed by Lowe and Thorneley,[67] it may not favor long-range ET. Intermediate ET pathways or hoping steps between P cluster and FeMoco are probably needed.

The existence of two clusters in the MoFe protein also explains the presence of more than two EADS because the two clusters could be simultaneously excited to their respective excited states and subsequently relax to ground states. This suggests that a parallel model might fit the data better. However, since the electronic states of MoFe protein are highly complicated due to the existence of two complex FeS clusters as well as the multiplicity of oxidation states that the two clusters can assume, it is very difficult to correctly decompose and assign the underlying spectral species. Nevertheless, the sequential analysis presented is sufficient for extracting the number of spectral species and roughly estimated their lifetimes, which are enough for the purpose of this study.

Comparison of the charge-transfer dynamics

Table 1 compares the lifetimes extracted from the sequential model analyses on the TA data of the four proteins. What is puzzling is that both *Pf*Rd and the MoFe protein exhibit significantly shorter lifetimes than Pdx and Fe protein. The fastest decaying system is the 1Fe-4S cluster in *Pf*Rd, which is three orders of magnitude faster than Pdx and Fe protein. The next fastest are the two clusters in the MoFe protein.

The overall lifetimes of Pdx and Fe protein are both on ns time scales, with that of the Fe protein slightly longer, which cannot be simply attributed to greater reorganization energy of the 4Fe-4S cluster (32 kJ/mol)[61] because it is actually very close to and even smaller than that of the 2Fe-2S cluster (36.8 kJ/mol).[28] As discussed above, the single long lifetime in the Fe protein might be due to the coupling of the six "virtual" pairs of 2Fe-2S clusters constituting the cubic 4Fe-4S cluster, which "smears" out the two long lifetimes in 2Fe-2S clusters. The reorganization energy of rubredoxin (~20 kJ/mol)[28, 61] is almost half of that of 2Fe-2S and 4Fe-4S clusters. Therefore the shorter lifetime of rubredoxin might be attributed to the smaller reorganization energy as proposed by Kennepohl and Solomon et al.[46] The increasing lifetimes from 1Fe to 4Fe clusters seems to suggest the MoFe protein should have even longer lifetime, which turns out to be the opposite. Considering that the two clusters in the MoFe protein are of considerably greater cluster complexity, the fast decaying kinetics is probably due to the greater electronic DOS in these two clusters and thus stronger electronic coupling between states. According to Sharma et al.,[36] even for clusters as simple as 2Fe-2S and 4Fe-4S clusters, there are several magnitudes of more electronic states than previously predicted. Therefore, the bigger clusters in MoFe protein probably have much more electronic states congested in the lower energy range compared to the simpler clusters.

We thus postulate that the cluster size has mainly two effects on the excited-state relaxation dynamics of FeS proteins: 1. Increased cluster size in general increases the reorganization energy of the cluster, and thus tend to increase the electronic state lifetimes. This effect may explain rubredoxin's extremely short excited state lifetime. However, direct relationship

between cluster size and reorganization energy is difficult to establish due to too many complicating factors as evidenced in 2Fe-2S and 4Fe-4S clusters. 2. Bigger cluster size andgreater cluster complexity increase the DOS and electronic coupling between states, thus decreasing the excited state lifetimes. From *Pf*Rd (1Fe-4S), Pdx (2Fe-2S), Fe protein (4Fe-4S), to P cluster (8Fe-7S), the main contributing factor to increased cluster complexity is the increased cluster size. However, for the P cluster and FeMoco of nitrogenase, the more complicated overall structures, the bigger structural changes upon redox reactions, and the inclusion of transition metal also contribute to the increased cluster complexity. These all lead to a greater DOS in these two clusters.

Concluding Comments

The electronic relaxation dynamics slow down with increasing cluster size from 1Fe to 4Fe clusters, and then become faster from 4Fe to 7 and 8 Fe clusters. The longer-lived CT states in 2Fe-2S clusters thus are not representative of the CT kinetics of all FeS clusters. Therefore, there is no direct relationship between cluster size and electronic relaxation dynamics in FeS clusters. The competition between the reorganization energy and DOS probably mediate their electronic relaxation lifetimes. In the efforts to construct novel materials or bio-functional proteins capable of utilizing CT properties, long-lived CT states are usually required. This suggests that 2Fe-2S or 4Fe-4S clusters, which have much longer excited states than the other clusters, are the optimal clusters to start with among FeS proteins. Due to the complexity of the P-cluster and the FeMoco, as well as the fact that their TA signals are a mixture of signals from both clusters, their CT properties are much more difficult to study than the smaller clusters with 1–4 irons. The present study contributes some efforts/insights towards a more complete understanding of the CT dynamics in these larger FeS clusters.

Supplementary Material

Refer to Web version on PubMed Central for supplementary material.

Acknowledgements

Abbreviations used in this paper:

FeS	iron-sulfur
FeMoco	iron-molybdenum cofactor
ET	electron transfer

HT	hole transfer
CT	charge transfer
***Pf*Rd**	*Pyrococcus furiosus* rubredoxin
***Dv*Rd**	*Desulfovibrio vulgaris* rubredoxin
Pdx	putidaredoxin
Rc6	*Rhodobacter capsulatus* ferredoxin VI
Fe	protein nitrogenase iron protein
MoFe	protein nitrogenase molybdenum-iron protein
EPR	electron paramagnetic resonance spectroscopy
NOPA	non-colinear optical parametric amplifier
TA	transient absorption
ICVS	impulsive coherent vibrational spectroscopy
BBO	beta barium borate
SHG	second harmonic generation
YAG	yttrium aluminum garnet
LMCT	ligand-to-metal charge transfer
ESA	excited state absorption
GSB	ground state bleaching
EADS	evolution associated difference spectra
SADS	species associated difference spectra
OD	optical density
CPM	cross phase modulation
DOS	density of states

References

[1]. Meyer J (2008) Iron-sulfur protein folds, iron-sulfur chemistry, and evolution, Journal of Biological Inorganic Chemistry 13, 157–170. [PubMed: 17992543]

[2]. Johnson DC, Dean DR, Smith AD, and Johnson MK (2005) Structure, function, and formation of biological iron-sulfur clusters, Annu. Rev. Biochem 74, 247–281. [PubMed: 15952888]

[3]. Bau R, Rees DC, Kurtz DM, Scott RA, Huang HS, Adams MWW, and Eidsness MK (1998) Crystal structure of rubredoxin from Pyrococcus furiosus at 0.95 angstrom resolution, and the structures of N-terminal methionine and formylmethionine variants of Pf Rd. Contributions of N-terminal interactions to thermostability, J. Biol. Inorg. Chem 3, 484–493.

[4]. Einsle O, Tezcan FA, Andrade SLA, Schmid B, Yoshida M, Howard JB, and Rees DC (2002) Nitrogenase MoFe-protein at 1.16 angstrom resolution: A central ligand in the FeMo-cofactor, Science 297, 1696–1700. [PubMed: 12215645]

[5]. Guigliarelli B, and Bertrand P (1999) Application of EPR spectroscopy to the structural and functional study of iron-sulfur proteins, Advances in Inorganic Chemistry, Vol 47 47, 421–497.

[6]. Ozaki Y, Nagayama K, Kyogoku Y, Hase T, and Matsubara H (1983) Resonance Raman-Spectroscopic Study on the Iron Sulfur Proteins Containing [2fe-2s] Clusters, FEBS Lett 152, 236–240.

[7]. Sainz G, Jakoncic J, Sieker LC, Stojanoff V, Sanishvili N, Asso M, Bertrand P, Armengaud J, and Jouanneau Y (2006) Structure of a [2Fe-2S] ferredoxin from Rhodobacter capsulatus likely involved in Fe-S cluster biogenesis and conformational changes observed upon reduction, J. Biol. Inorg. Chem 11, 235–246. [PubMed: 16402206]

[8]. Brown KA, Dayal S, Ai X, Rumbles G, and King PW (2010) Controlled Assembly of Hydrogenase-CdTe Nanocrystal Hybrids for Solar Hydrogen Production, J. Am. Chem. Soc 132, 9672–9680.solomon [PubMed: 20583755]

[9]. Brown KA, Harris DF, Wilker MB, Rasmussen A, Khadka N, Hamby H, Keable S, Dukovic G, Peters JW, Seefeldt LC, and King PW (2016) Light-driven dinitrogen reduction catalyzed by a CdS:nitrogenase MoFe protein biohybrid, Science 352, 448–450. [PubMed: 27102481]

[10]. Kim CS, and Jung J (1992) Iron Sulfur Centers as Endogenous Blue-Light Sensitizers in Cells - a Study with an Artificial Nonheme Iron Protein, Photochem. Photobiol 56, 63–68. [PubMed: 1508984]

[11]. Hochkoeppler A, Zannoni D, Ciurli S, Meyer TE, Cusanovich MA, and Tollin G (1996) Kinetics of photo-induced electron transfer from high-potential iron-sulfur protein to the photosynthetic reaction center of the purple phototroph Rhodoferax fermentans, Proc. Natl. Acad. Sci. U.S.A 93, 6998–7002. [PubMed: 8692932]

[12]. Adam D, Bosche L, Castaneda-Losada L, Winkler M, Apfel P, and Happe T (2017) Sunlight-Dependent Hydrogen Production by Photosensitizer/Hydrogenase Systems, Chemsuschem 10, 894–902. [PubMed: 27976835]

[13]. Wang WG, Rauchfuss TB, Bertini L, and Zampella G (2012) Unsensitized Photochemical Hydrogen Production Catalyzed by Diiron Hydrides, J. Am. Chem. Soc 134, 4525–4528. [PubMed: 22364563]

[14]. Engstrom G, Xiao KH, Yu CA, Yu L, Durham B, and Millett F (2002) Photoinduced electron transfer between the Rieske iron-sulfur protein and cytochrome c(1) in the Rhodobacter sphaeroides cytochrome bc(1) complex - Effects of pH, temperature, and driving force, J. Biol. Chem 277, 31072–31078. [PubMed: 12045199]

[15]. Jenney FE, and Adams MWW (2001) Rubredoxin from Pyrococcus furiosus, Hyperthermophilic Enzymes, Pt C 334, 45–55.

[16]. Hugenholtz J, and Ljungdahl LG (1990) Amino-Acid-Transport in Membrane-Vesicles of Clostridium-Thermoautotrophicum, FEMS Microbiol. Lett 69, 117–121.

[17]. Seki Y, Seki S, Satoh M, Ikeda A, and Ishimoto M (1989) Rubredoxin from Clostridium-Perfringens - Complete Amino-Acid Sequence and Participation in Nitrate Reduction, J. Biochem 106, 336–341. [PubMed: 2553684]

[18]. van Beilen JB, Neuenschwander M, Smits THM, Roth C, Balada SB, and Witholt B (2002) Rubredoxins involved in alkane oxidation, J. Bacteriol 184, 1722–1732. [PubMed: 11872724]

[19]. Auchere F, Sikkink R, Cordas C, Raleiras P, Tavares P, Moura I, and Moura JJG (2004) Overexpression and purification of Treponema pallidum rubredoxin; kinetic evidence for a superoxide-mediated electron transfer with the superoxide reductase neelaredoxin, J. Biol. Inorg. Chem 9, 839–849. [PubMed: 15328557]

[20]. Hernandez G, Jenney FE, Adams MWW, and LeMaster DM (2000) Millisecond time scale conformational flexibility in a hyperthermophile protein at ambient temperature, Proc. Natl. Acad. Sci. U.S.A 97, 3166–3170. [PubMed: 10716696]

[21]. Mao Z, Carroll EC, Kim PW, Cramer SP, and Larsen DS (2017) Ultrafast Charge Transfer Dynamics in the Iron-Sulfur Complex of Rhodobacter Capsulatus Ferredoxin VI, J. Phys. Chem. Lett

[22]. Katagiri M, Ganguli BN, and Gunsalus IC (1968) A Soluble Cytochrome P-450 Functional in Methylene Hydroxylation, J. Biol. Chem 243, 3543-&. [PubMed: 4297783]

[23]. Sevrioukova IF, Garcia C, Li HY, Bhaskar B, and Poulos TL (2003) Crystal structure of putidaredoxin, the [2Fe-2S] component of the P450cam monooxygenase system from Pseudomonas putida, J. Mol. Biol 333, 377–392. [PubMed: 14529624]

[24]. Boratyn GM, Camacho C, Cooper PS, Coulouris G, Fong A, Ma N, Madden TL, Matten WT, McGinnis SD, Merezhuk Y, Raytselis Y, Sayers EW, Tao T, Ye J, and Zaretskaya I (2013) BLAST: a more efficient report with usability improvements, Nucleic Acids Res 41, W29–W33. [PubMed: 23609542]

[25]. Dauter Z, Wilson KS, Sieker LC, Meyer J, and Moulis JM (1997) Atomic resolution (0.94 angstrom) structure of Clostridium acidurici ferredoxin. Detailed geometry of [4Fe-4S] clusters in a protein, Biochemistry 36, 16065–16073. [PubMed: 9405040]

[26]. Hoffman BM, Lukoyanov D, Yang ZY, Dean DR, and Seefeldt LC (2014) Mechanism of Nitrogen Fixation by Nitrogenase: The Next Stage, Chem. Rev 114, 4041–4062. [PubMed: 24467365]

[27]. Peters JW, Lanzilotta WN, Lemon BJ, and Seefeldt LC (1998) X-ray crystal structure of the Fe-only hydrogenase (CpI) from Clostridium pasteurianum to 1.8 angstrom resolution, Science 282, 1853–1858. [PubMed: 9836629]

[28]. Sigfridsson E, Olsson MHM, and Ryde U (2001) Inner-sphere reorganization energy of iron-sulfur clusters studied with theoretical methods, Inorg. Chem 40, 2509–2519. [PubMed: 11350228]

[29]. Maskos Z, and Hales BJ (2003) Photo-lability of CO bound to mo-nitrogenase from Azotobacter vinelandii, J. Inorg. Biochem 93, 11–17. [PubMed: 12538048]

[30]. Yan LF, Dapper CH, George SJ, Wang HX, Mitra D, Dong WB, Newton WE, and Cramer SP (2011) Photolysis of Hi-CO Nitrogenase - Observation of a Plethora of Distinct CO Species Using Infrared Spectroscopy, Eur. J. Inorg. Chem, 2064–2074. [PubMed: 27630531]

[31]. Christiansen J, Goodwin PJ, Lanzilotta WN, Seefeldt LC, and Dean DR (1998) Catalytic and biophysical properties of a nitrogenase apo-MoFe protein produced by a nifB-deletion mutant of Azotobacter vinelandii, Biochemistry 37, 12611–12623. [PubMed: 9730834]

[32]. Christiansen J, Cash VL, Seefeldt LC, and Dean DR (2000) Isolation and characterization of an acetylene-resistant nitrogenase, J. Biol. Chem 275, 11459–11464. [PubMed: 10753963]

[33]. Carroll EC, Compton OC, Madsen D, Osterloh FE, and Larsen DS (2008) Ultrafast carrier dynamics in exfoliated and functionalized calcium niobate nanosheets in water and methanol, J. Phys. Chem. C 112, 2394–2403.

[34]. Noodleman L, and Baerends EJ (1984) Electronic-Structure, Magnetic-Properties, Electron-Spin-Resonance, and Optical-Spectra for 2-Fe Ferredoxin Models by Lcao-X-Alpha Valence Bond Theory, J. Am. Chem. Soc 106, 2316–2327.

[35]. Larsen DS (2002) A small volume, rapid translation cryostat insert constructed from commercial components for the detection of ultrafast optical signals, Rev. Sci. Instrum 73, 1325–1328.

[36]. Sharma S, Sivalingam K, Neese F, and Chan GKL (2014) Low-energy spectrum of iron-sulfur clusters directly from many-particle quantum mechanics, Nat. Chem 6, 927–933. [PubMed: 25242489]

[37]. Stephens PJ, Mckenna CE, Smith BE, Nguyen HT, Mckenna MC, Thomson AJ, Devlin F, and Jones JB (1979) Circular-Dichroism and Magnetic Circular-Dichroism of Nitrogenase Proteins, Proc. Natl. Acad. Sci. U.S.A 76, 2585–2589. [PubMed: 379860]

[38]. Shah VK, and Brill WJ (1973) Nitrogenase .4. Simple Method of Purification to Homogeneity of Nitrogenase Components from Azotobacter-Vinelandil, Biochim. Biophys. Acta 305, 445–454. [PubMed: 4354875]

[39]. Arragain S, Garcia-Serres R, Blondin G, Douki T, Clemancey M, Latour JM, Forouhar F, Neely H, Montelione GT, Hunt JF, Mulliez E, Fontecave M, and Atta M (2010) Post-translational Modification of Ribosomal Proteins Structural and Functional Characterization of RimO From Thermotoga Maritima, A Radical S-Adenosylmethionine Methylthiotransferase, J. Biol. Chem 285, 5792–5801. [PubMed: 20007320]

[40]. Kovalenko SA, Dobryakov AL, Ruthmann J, and Ernsting NP (1999) Femtosecond spectroscopy of condensed phases with chirped supercontinuum probing, Phys. Rev. A 59, 2369–2384.

[41]. Ekvall K, van der Meulen P, Dhollande C, Berg LE, Pommeret S, Naskrecki R, and Mialocq JC (2000) Cross phase modulation artifact in liquid phase transient absorption spectroscopy, J. Appl. Phys 87, 2340–2352.

[42]. Lorenc M, Ziolek M, Naskrecki R, Karolczak J, Kubicki J, and Maciejewski A (2002) Artifacts in femtosecond transient absorption spectroscopy, Applied Physics B-Lasers and Optics 74, 19–27.

[43]. van Stokkum IHM, Larsen DS, and van Grondelle R (2004) Global and target analysis of time-resolved spectra, Biochim. Biophys. Acta, Bioenerg 1657, 82–104.

[44]. Holzwarth AR (1996) Data Analysis of Time-Resolved Measurements, In Biophysical techniques in photosynthesis (Amesz J, and Hoff AJ, Eds.), pp 75–92, Springer, Dordrecht, The Netherlands.

[45]. Kennepohl P, and Solomon EI (2003) Electronic structure contributions to electron-transfer reactivity in iron-sulfur active sites: 1. Photoelectron spectroscopic determination of electronic relaxation, Inorg. Chem 42, 679–688. [PubMed: 12562181]

[46]. Kennepohl P, and Solomon EI (2003) Electronic structure contributions to electron-transfer reactivity in iron-sulfur active sites: 3. Kinetics of electron transfer, Inorg. Chem 42, 696–708. [PubMed: 12562183]

[47]. Kennepohl P, and Solomon EI (2003) Electronic structure contributions to electron-transfer reactivity in iron-sulfur active sites: 2. Reduction potentials, Inorg. Chem 42, 689–695. [PubMed: 12562182]

[48]. Yang Y, Beck BW, Shenoy VS, and Ichiye T (1993) Aqueous Solvation of a Rubredoxin Redox Site Analog - a Molecular-Dynamics Simulation, J. Am. Chem. Soc 115, 7439–7444.

[49]. Im SG, and Sykes AG (1996) Kinetic studies on the redox reactions of Clostridium pasteurianum rubredoxin, J Chem Soc Dalton, 2219–2222.

[50]. Tan ML, Bizzarri AR, Xiao YM, Cannistraro S, Ichiye T, Manzoni C, Cerullo G, Adams MWW, Jenney FE, and Cramer SP (2007) Observation of terahertz vibrations in Pyrococcus furiosus rubredoxin via impulsive coherent vibrational spectroscopy and nuclear resonance vibrational spectroscopy - interpretation by molecular mechanics, J. Inorg. Biochem 101, 375–384. [PubMed: 17204331]

[51]. Gray HB, and Winkler JR (2015) Hole hopping through tyrosine/tryptophan chains protects proteins from oxidative damage, Proc. Natl. Acad. Sci. U.S.A 112, 10920–10925. [PubMed: 26195784]

[52]. Holden HM, Jacobson BL, Hurley JK, Tollin G, Oh BH, Skjeldal L, Chae YK, Cheng H, Xia B, and Markley JL (1994) Structure-Function Studies of [2fe-2s] Ferredoxins, J. Bioenerg. Biomembr 26, 67–88. [PubMed: 8027024]

[53]. Dugad LB, Lamar GN, Banci L, and Bertini I (1990) Identification of Localized Redox States in Plant-Type 2-Iron Ferredoxins Using the Nuclear Overhauser Effect, Biochemistry 29, 2263–2271. [PubMed: 2110829]

[54]. Hannemann F, Rottmann M, Schiffler B, Zapp J, and Bernhardt R (2001) The loop region covering the iron-sulfur cluster in bovine adrenodoxin comprises a new interaction site for redox partners, J. Biol. Chem 276, 1369–1375. [PubMed: 11013256]

[55]. Stayton PS, and Sligar SG (1991) Structural Microheterogeneity of a Tryptophan Residue Required for Efficient Biological Electron-Transfer between Putidaredoxin and Cytochrome-P-450cam, Biochemistry 30, 1845–1851. [PubMed: 1993199]

[56]. Kuznetsov VY, Poulos TL, and Sevrioukova IF (2006) Putidaredoxin-to-cytochrome P450cam electron transfer: Differences between the two reductive steps required for catalysis, Biochemistry 45, 11934–11944. [PubMed: 17002293]

[57]. Kurnikov IV (2000) HARLEM molecular modeling package, v 1.0, Department of Chemistry, University of Pittsburgh, Pittsburgh, PA, USA.

[58]. Roitberg A, Holden M, Mayhew M, Beratan D, Kurnikov I, and Vilker V (1998) Binding and electron transfer between putidaredoxin and cytochrome P450cam. Theory and experiments., Abstr Pap Am Chem S 215, U236–U237.

[59]. Sevrioukova IF, Poulos TL, and Churbanova IY (2010) Crystal Structure of the Putidaredoxin Reductase.Putidaredoxin Electron Transfer Complex, J. Biol. Chem 285, 13616–13620. [PubMed: 20179327]

[60]. Byrdin M, Sartor V, Eker APM, Vos MH, Aubert C, Brettel K, and Mathis P (2004) Intraprotein electron transfer and proton dynamics during photoactivation of DNA photolyase from E-coli: review and new insights from an "inverse" deuterium isotope effect, Biochim. Biophys. Acta, Bioenerg 1655, 64–70.

[61]. Reynolds JG, Coyle CL, and Holm RH (1980) Electron Exchange Kinetics of [Fe4s4(Sr)4]2--[Fe4s4(Sr)4]3-and [Fe4se4(Sr)4]2--[Fe4se4(Sr)4]3-Systems - Estimates of the Intrinsic Self-Exchange Rate-Constant of 4-Fe Sites in Oxidized and Reduced Ferredoxins, J. Am. Chem. Soc 102, 4350–4355.

[62]. Aizman A, and Case DA (1982) Electronic-Structure Calculations on Active-Site Models for 4-Fe, 4-S Iron Sulfur Proteins, J. Am. Chem. Soc 104, 3269–3279.

[63]. Noodleman L, Norman JG, Osborne JH, Aizman A, and Case DA (1985) Models for Ferredoxins - Electronic-Structures of Iron Sulfur Clusters with One, 2, and 4 Iron Atoms, J. Am. Chem. Soc 107, 3418–3426.

[64]. Yang ZY, Danyal K, and Seefeldt LC (2011) Mechanism of Mo-Dependent Nitrogenase, Nitrogen Fixation: Methods and Protocols 766, 9–29.

[65]. Fermi E (1950) Nuclear Physics, University of Chicago Press, Chicago, USA.

[66]. Peters JW, Fisher K, Newton WE, and Dean DR (1995) Involvement of the P Cluster in Intramolecular Electron Transfer within the Nitrogenase MoFe protein, The Journal of Biological Chemistry 270, 27007–27013. [PubMed: 7592949]

[67]. Thorneley RNF, and Lowe D (1985) Kinetics and mechanism of the nitrogenase enzyme system, In Molybdenum Enzymes (Spiro TG, Ed.), pp 221–284, Wiley, New York, NY, USA.
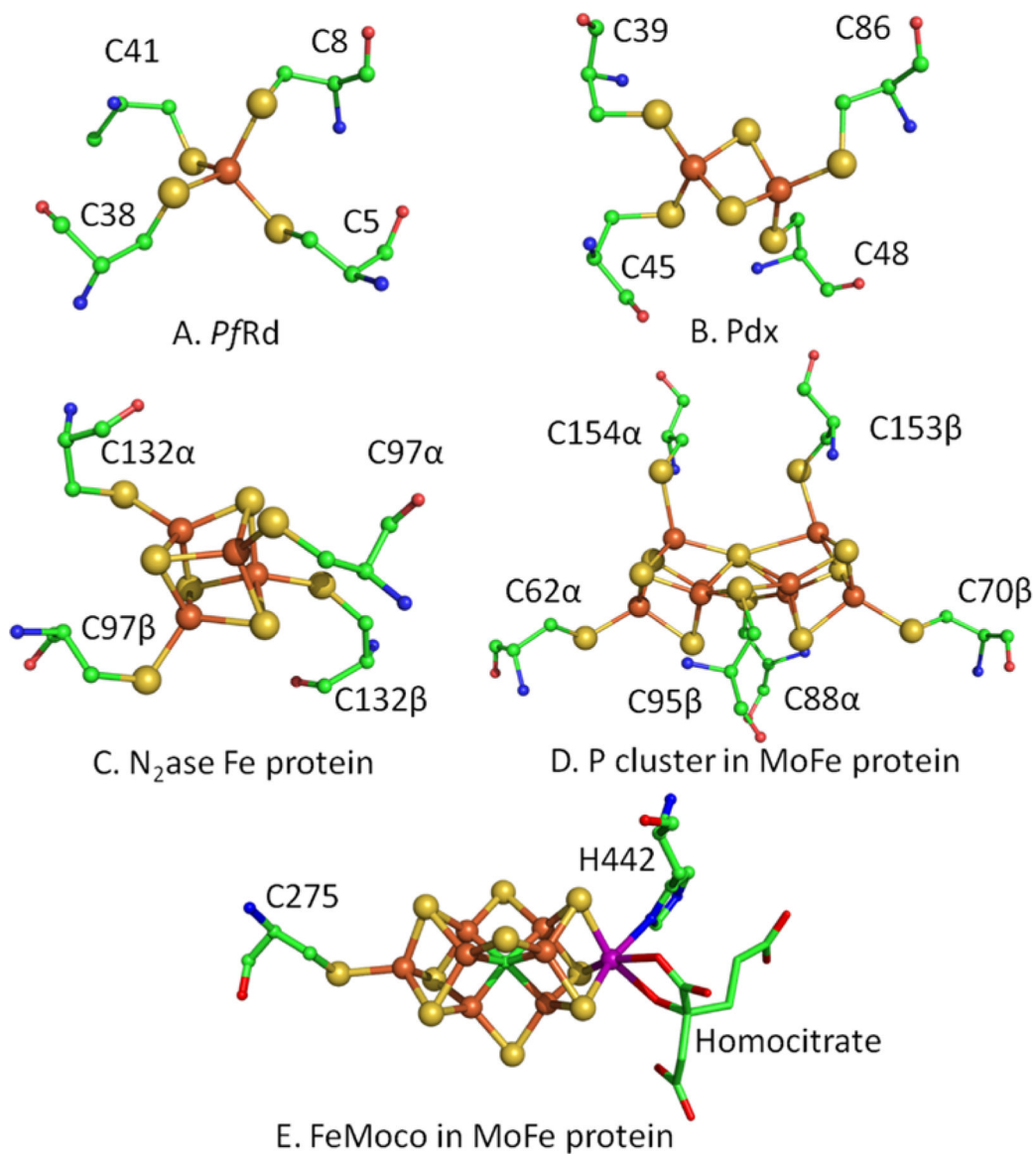
Figure 1.
Active site structures of (A) *Pf*Rd, (B) Pdx, (C) Nitrogenase Fe protein, (D) 8Fe-7S P-cluster in nitrogenase MoFe protein, and (E) 7Fe-9S-1Mo cofactor (FeMoco) in nitrogenase MoFe protein. Color coding: Fe (brick), S (yellow), C (green), N (blue), O (red), Mo (purple). PDB codes: 1BRF (*Pf*Rd), 1PUT (Pdx), 1FP6 (nitrogenase Fe protein), 3MIN (nitrogenase MoFe protein: P cluster and FeMoco).
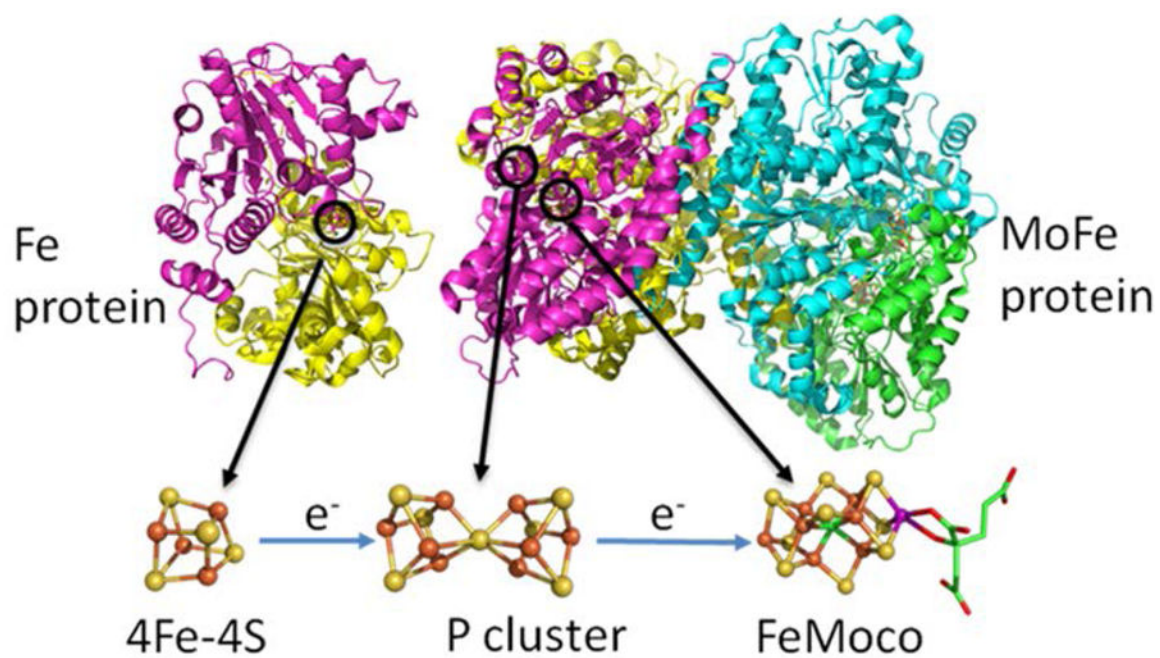
Figure 2.
Electron transfer chain in nitrogenase. PDB codes: 1FP6 (nitrogenase Fe protein), 3MIN (nitrogenase MoFe protein).
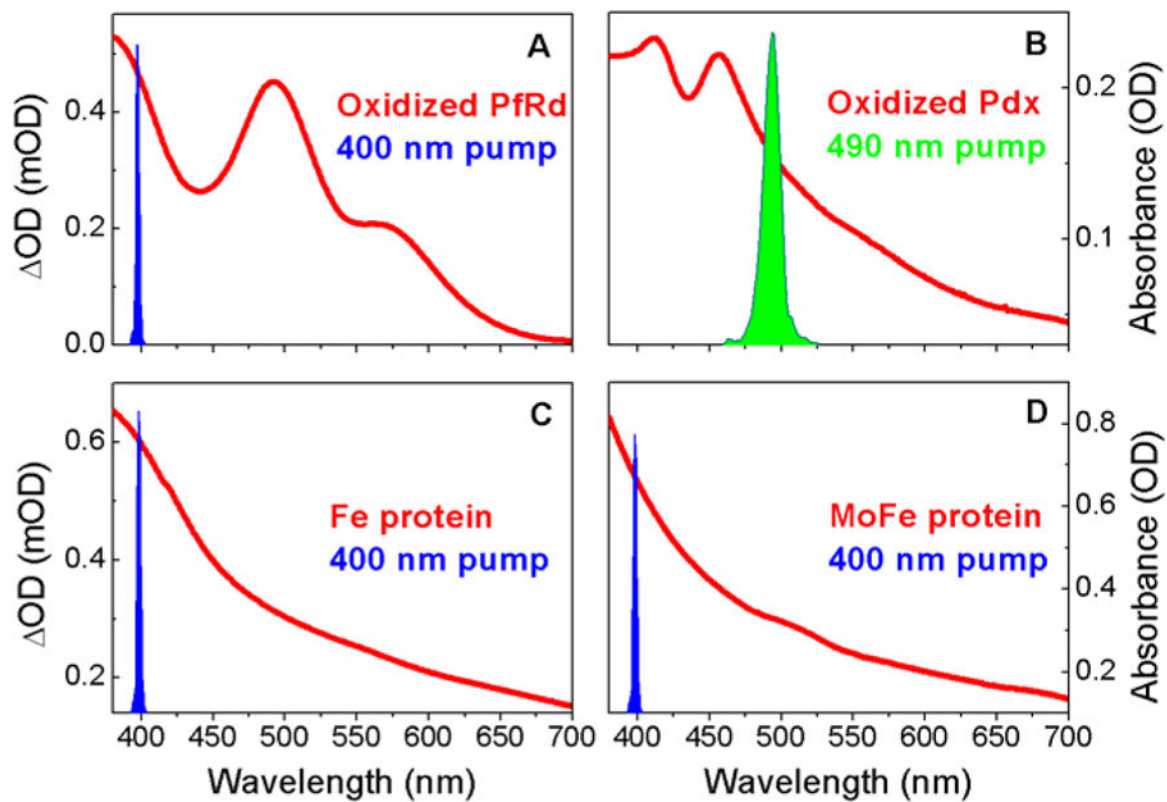
Figure 3.
Static absorption spectra of oxidized *Pf*Rd (A), oxidized Pdx (B), nitrogenase Fe protein (C) and nitrogenase MoFe protein (D), together with the respective pump/excitation laser spectra.
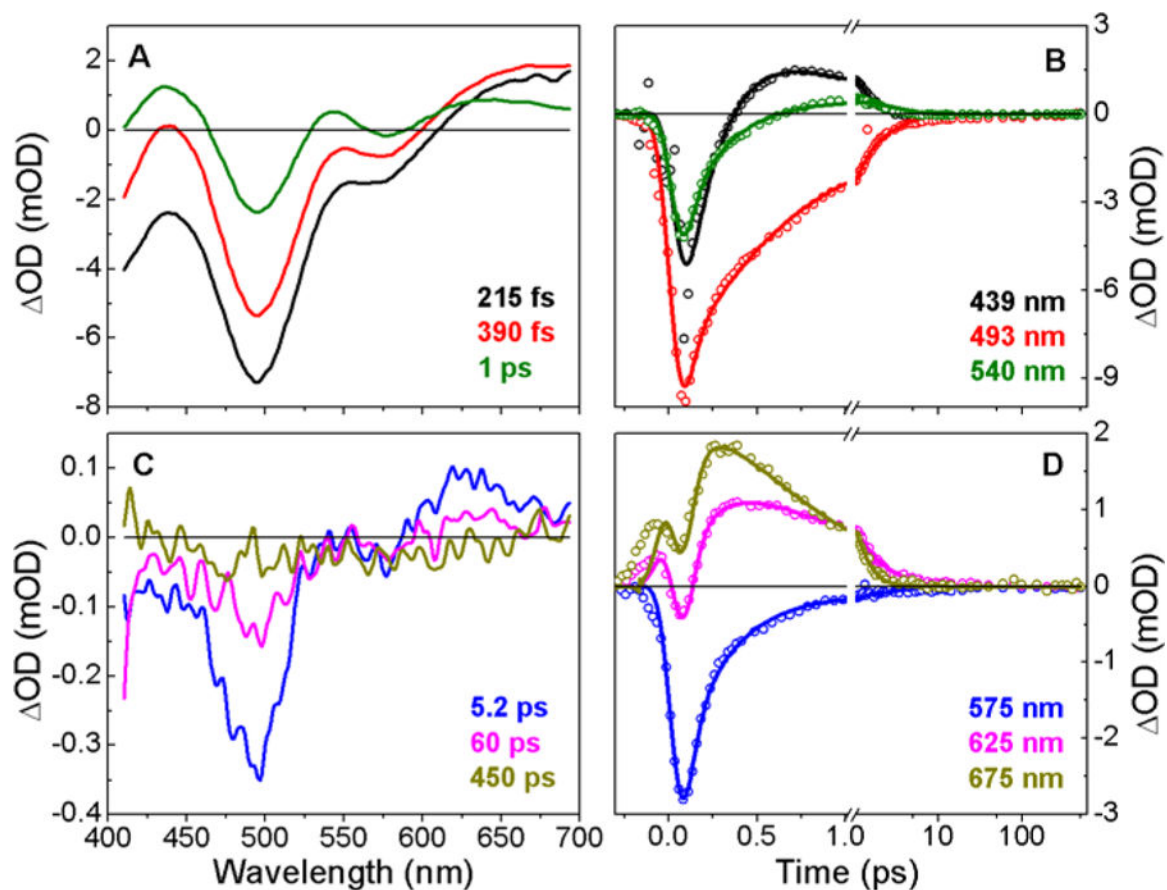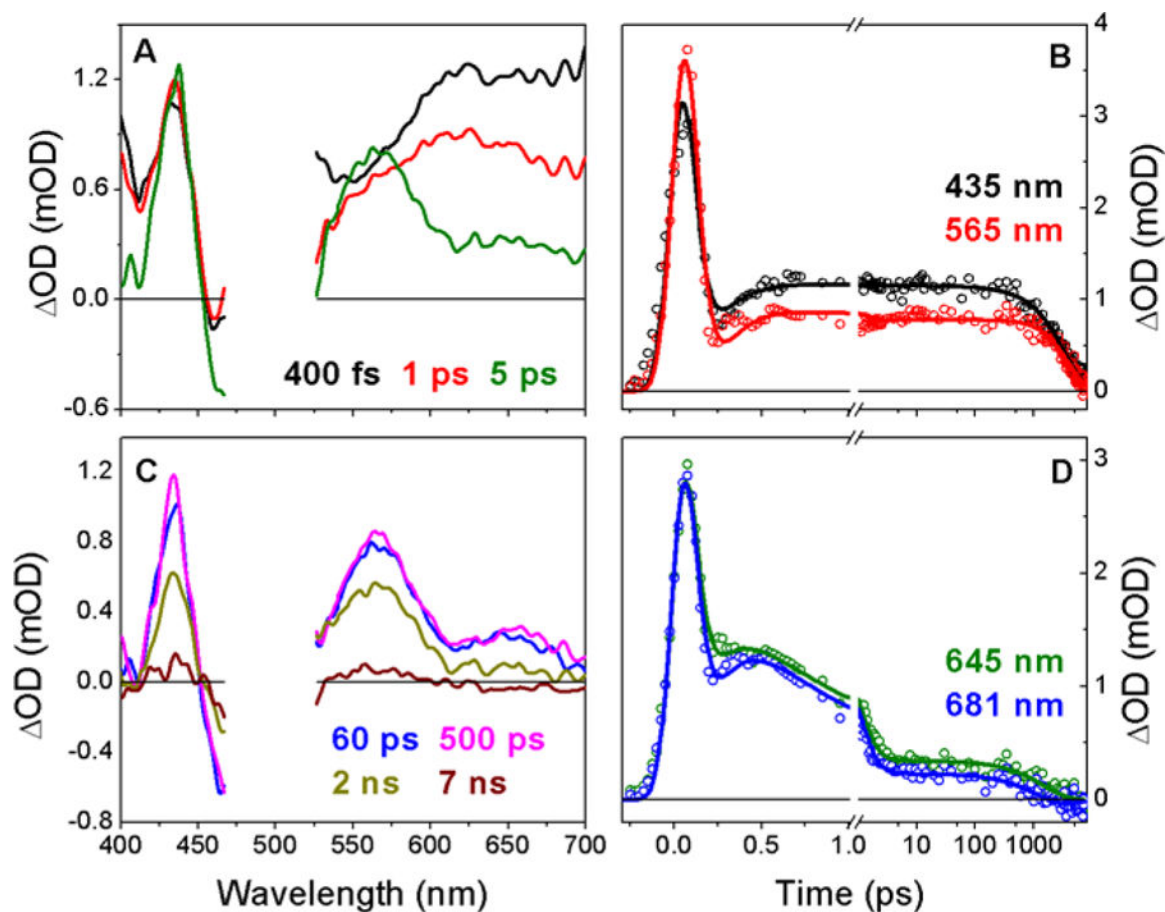
Figure 4.
TA spectra of *Pf*Rd (1Fe-4S site) at select probe times (A and C), together with kinetics at select wavelengths (B and D). The open circles represent the fits to the TA data using a four-compartment sequential model. Dispersion at different wavelengths have been adjusted to bring the beginning of the kinetics at the same time zero. The data after 1 ps are on log time scale. Excitation at 400 nm.
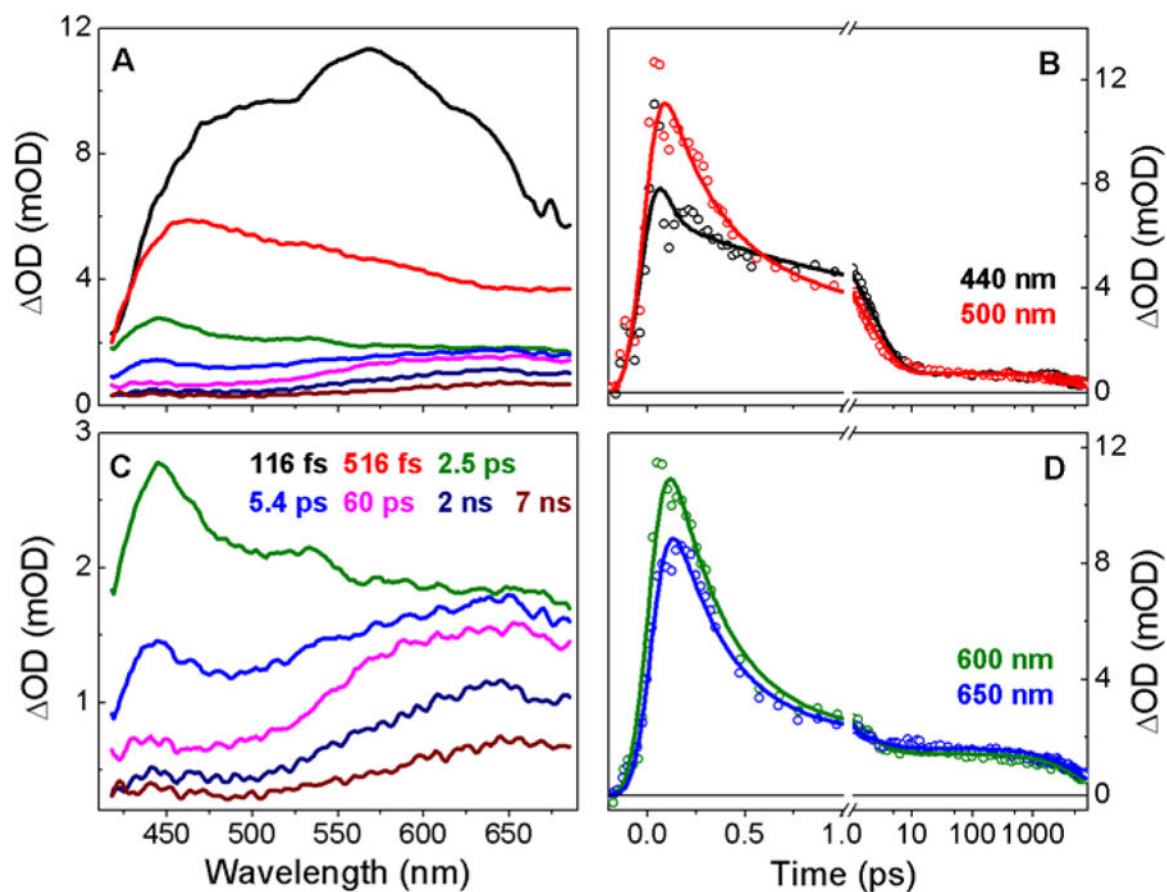
Figure 5.
TA spectra of Pdx (2Fe-2S cluster) at select probe times (A and C), together with kinetics at select wavelengths (B and D). The data perturbed by the scattering of the 490 nm excitation light have been removed from the spectra. The open circles represent the fits to the TA data using a six-compartment sequential model. Dispersion at different wavelengths have been adjusted to bring the beginning of the kinetics at the same time zero. The data after 1 ps are on log time scale. Excitation at 490 nm.
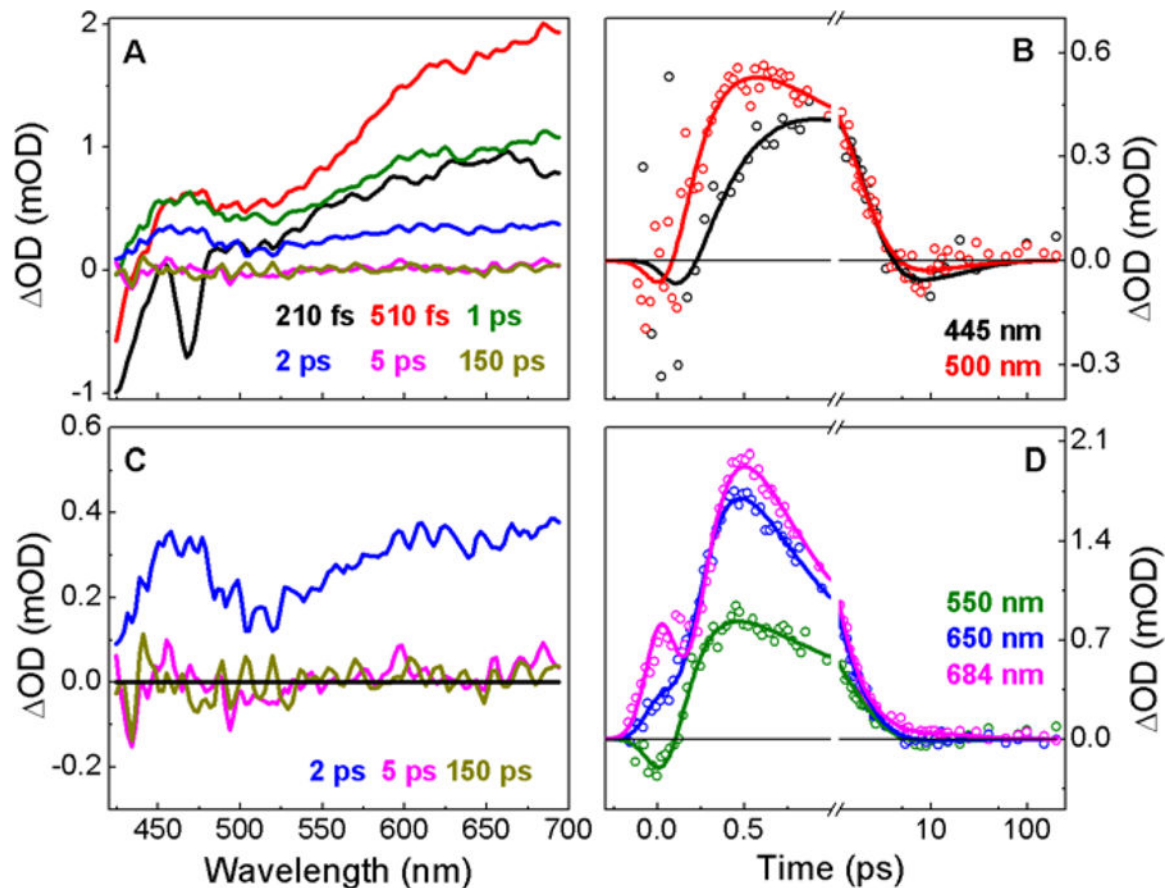
Figure 6.
TA spectra of nitrogenase Fe protein (4Fe-4S cluster) at select probe times (A and C), together with kinetics at select wavelengths (B and D). The open circles represent the fits to the TA data using a four-compartment sequential model. Dispersion at different wavelengths has been adjusted to bring the beginning of the kinetics at the same time zero. The data after 1 ps are on log time scale. Excitation at 400 nm.
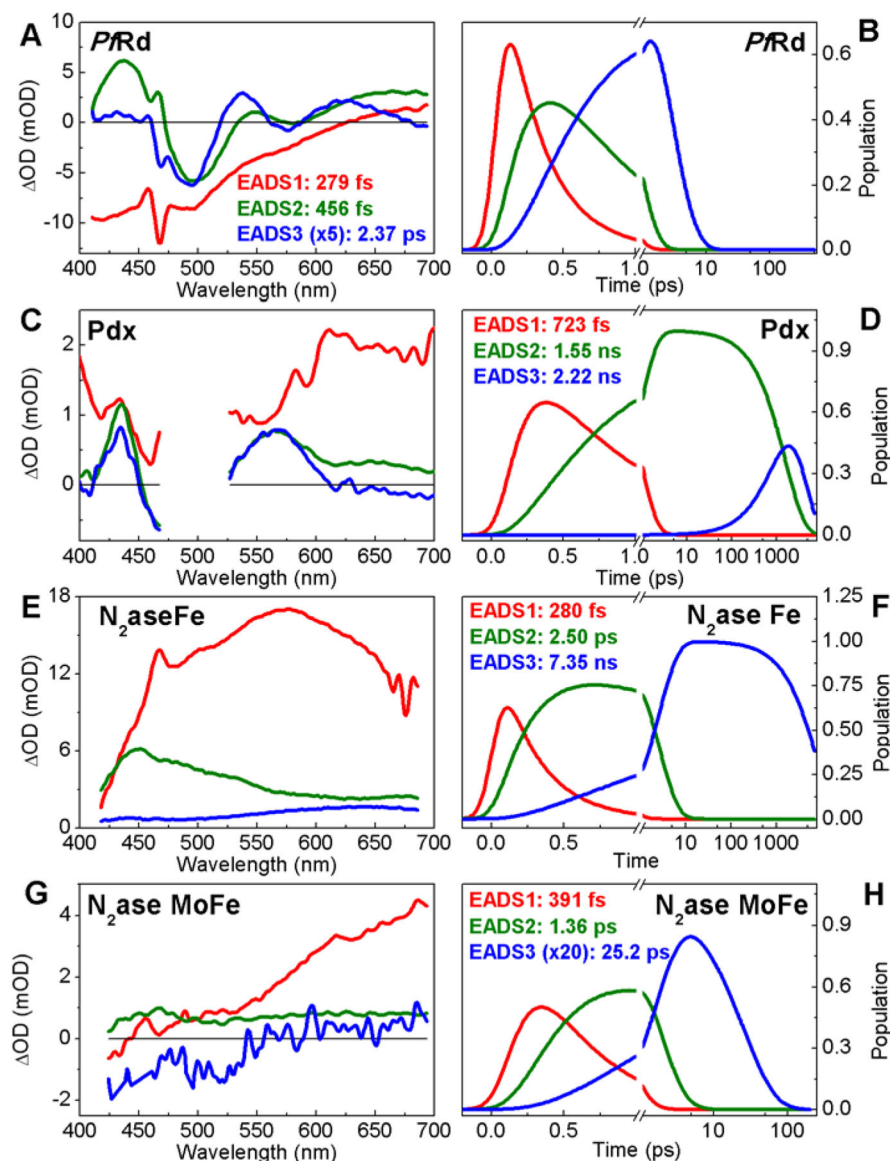
Figure 7.
TA spectra of nitrogenase MoFe protein (7Fe-9S-1Mo cluster) at select probe times (A and C), together with kinetics at select wavelengths (B and D). The open circles represent the fits to the TA data using a five-compartment sequential model. Dispersion at different wavelengths have been adjusted to bring the beginning of the kinetics at the same time zero. The data after 1 ps are on log time scale. Excitation at 400 nm.

Figure 8.

(A & B) Extracted EADS 1–3 (A) and corresponding population profile (B) for the fit of the sequential model in Figure S2 to the TA data of *Pf*Rd (Figure 4). EADS3 was scaled up five-fold. Short lived components used to fit the cross phase modulation (CPM) and water Raman signals[42] are shown in Figure S3. *(C & D)* Extracted EADS (C) and corresponding population profile (D) for the fit of the sequential model in Figure S3 to the TA data of Pdx (Figure 5). Shorted lived components used to fit the CPM artifact and water Raman signals is shown in Figure S3. *(E & F)* Extracted EADS (E) and corresponding population profile (F) for the fit of the sequential model in Figure S4 to the TA data of nitrogenase (N2ase) Fe protein (Figure 6). The short-lived component used to fit the CPM and water Raman signals is shown in Figure S4. *(G & H)* Extracted EADS (G) and corresponding polulation profile (H) for the fit of the sequential model in Figure S5 to the TA data of N2ase MoFe protein (Figure 7). The EADS3 was scaled up 20-fold. The short-lived components used to fit the

CPM and water Raman signals are shown in Figure S5. The population profiles after 1 ps are on log time scale.
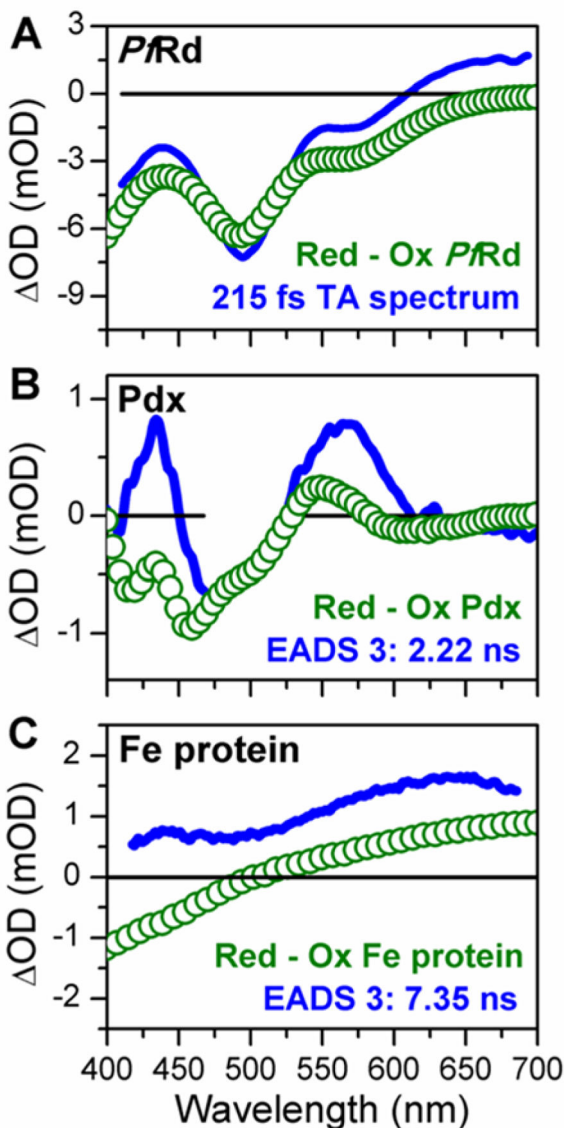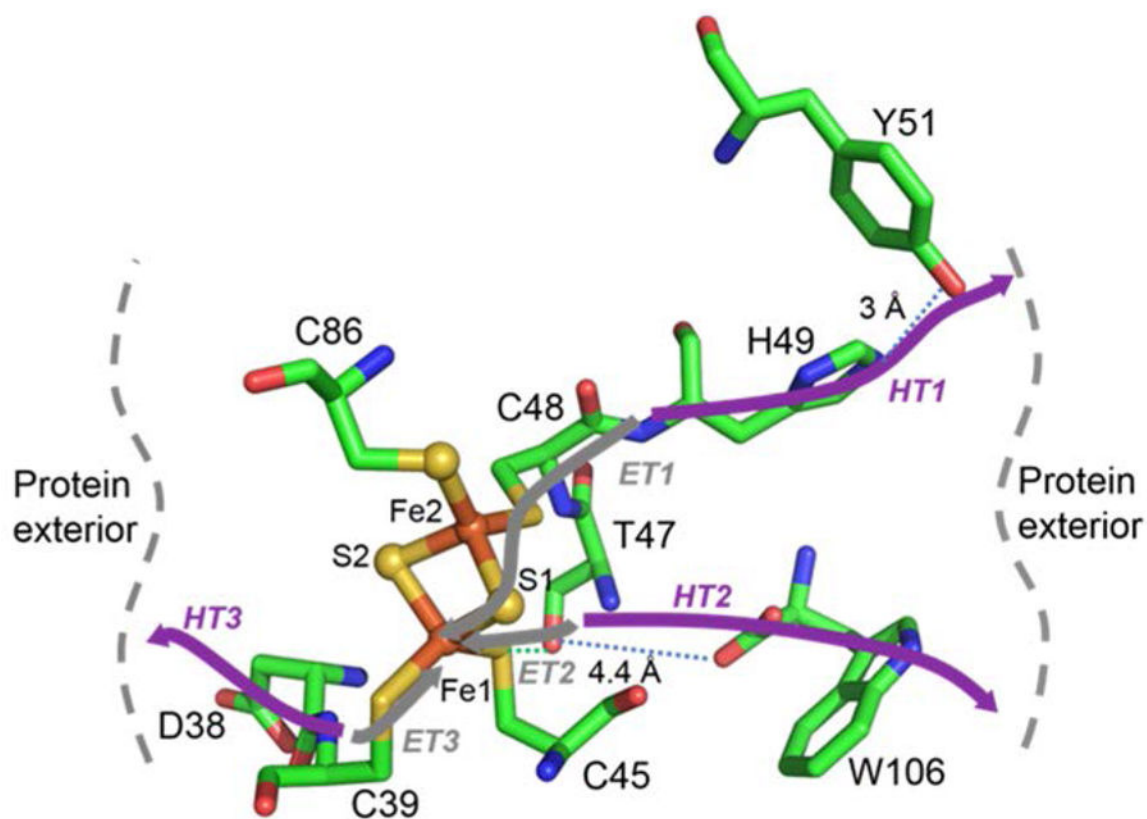
Figure 9.
(A) TA spectrum of *Pf*Rd at 215 fs (blue solid curve) compared with the static difference absorption spectrum (olive, open circles) obtained by subtracting the absorption spectrum of oxidized (Ox) *Pf*Rd from that of reduced (Red) *Pf*Rd. (B). EADS3 of Pdx (blue solid curve) compared with the static difference absorption spectrum (olive, open circles) obtained by subtracting the absorption spectrum of oxidized (Ox) Pdx from that of reduced (Red) Pdx. The data perturbed by the scattering of the 490 nm excitation laser pulse have been excised from the EADS3. (C). EADS3 of nitrogenase Fe protein (blue solid curve) compared with the static difference absorption spectrum (olive, open circles) obtained by subtracting the absorption spectrum of oxidized (Ox) Fe protein from that of sodium dithionite reduced (Red) Fe protein.

Scheme 1.
Potential electron-transfer (ET, gray arrows) and hole-transfer (HT, purple arrows) pathways in Pdx.

Table 1.

Lifetimes extracted from the sequential EADS analyses in Figure 8

Population	*Pf*Rd	Pdx	Fe protein	MoFe protein
EADS1	279 fs	723 fs	280 fs	391 fs
EADS2	456 fs	1.55 ns	2.50 ps	1.36 ps
EADS3	2.37 ps	2.22 ns	7.35 ns	25.2 ps